

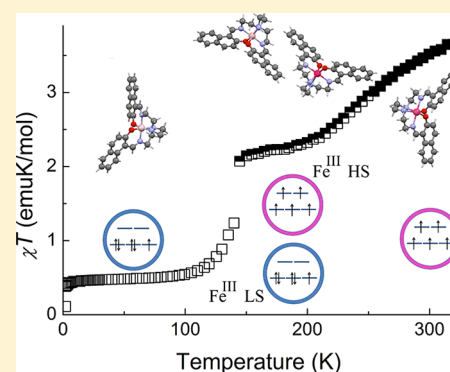
# [Fe(nsal<sub>2</sub>trien)]SCN, a New Two-Step Iron(III) Spin Crossover Compound, with Symmetry Breaking Spin-State Transition and an Intermediate Ordered State

Bruno J. C. Vieira, Joana T. Coutinho, Isabel C. Santos, Laura C. J. Pereira, João C. Waerenborgh, and Vasco da Gama\*

UCQR, IST/ITN, Instituto Superior Técnico, Universidade Técnica de Lisboa, CFMC-UL, 2686-953 Sacavém, Portugal

## Supporting Information

**ABSTRACT:** We report the synthesis of the iron(III) complex of the hexadentate Schiff base ligand nsal<sub>2</sub>trien obtained from the condensation of triethylenetetramine and 2 equiv. of 2-hydroxy-1-naphthaldehyde. The study of the salt [Fe(nsal<sub>2</sub>trien)]SCN (**1**) by magnetic susceptibility measurements and Mössbauer spectroscopy reveals a rather unique behavior that displays thermally induced spin crossover (SCO) with two well-separated steps at 250 (gradual transition) and 142 K (steep transition). Single crystal X-ray structures were obtained at 294, 150, and 50 K, for the high spin (HS), intermediate (Int), and low spin (LS) phases. The HS and LS phases are isostructural, and based on a single Fe<sup>III</sup> site (either HS or LS) an unusual symmetry break occurs in the transition to the Int ordered phase, where the unit cell includes two distinct Fe<sup>III</sup> sites and is based on a repetition of the [HS–LS] motif. The two-step SCO behavior of **1** must result from the existence of structural constraints preventing the full conversion HS ↔ LS in a single step.

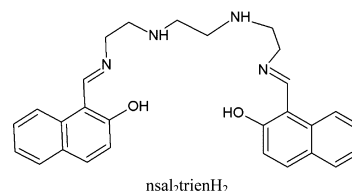


## INTRODUCTION

The spin crossover (SCO) phenomenon is found in a variety of 3d<sup>4</sup>–3d<sup>7</sup> transition metal complexes and has been extensively studied in past decades.<sup>1,2</sup> In these complexes, the spin state of the transition metal can be reversibly switched between the low-spin (LS) and high-spin (HS) states by the application of an external perturbation (such as temperature, pressure, magnetic field, light irradiation). The bistability between the HS and LS states is quite promising for the application as molecular memories and switches, as it is associated with changes in the physical properties (crystal structure, magnetism, color, etc.) and its progress can be monitored using a variety of techniques.<sup>1–3</sup> The SCO behavior is often characterized by a “transition curve” that describes the relative concentrations of the HS (or LS) state with temperature. Most frequently, these curves exhibit a single step thermal dependence, but in recent years examples of two-step transitions have been observed, where HS ↔ LS transformation occurs through an intermediate (Int) phase. In these systems, there is an increase in the switching possibilities as three states become available, which enables a larger information storage capacity.

In mononuclear complexes, two-step transitions occur frequently in the presence of two (or more) different lattice sites, with distinct SCO transition temperatures for each site.<sup>4</sup> However, in a few situations the SCO process in these complexes was found to be associated with a symmetry breaking in the crystal structure.<sup>5</sup> This was observed for the first time in [Fe<sup>II</sup>(2-pic)<sub>3</sub>]Cl<sub>2</sub>·EtOH (pic = 2-picolyamine),<sup>5a</sup> where

the (single site) HS and LS isostructural phases are separated by an Int phase with two distinct Fe<sup>II</sup> sites (one in HS and the other LS). Recently, a similar situation was reported for the first time in an Fe<sup>III</sup> complex,<sup>5d</sup> where a symmetry break was observed, but no re-entrant LS phase could be detected. Here, we report the first example of a two-step SCO mononuclear Fe<sup>III</sup> complex, [Fe(nsal<sub>2</sub>trien)]SCN (**1**), with structural symmetry breaking in the Int phase (with the doubling of the unit cell) and a “re-entrant” behavior as the LS crystal structure is isostructural to the one in the HS phase. The hexadentate nsal<sub>2</sub>trien ligand (see scheme below) was obtained by condensation of triethylenetetramine with 2-hydroxy-1-naphthaldehyde.



## RESULTS AND DISCUSSION

The temperature dependence of the  $\chi T$  product ( $\chi$  is the molar paramagnetic susceptibility and  $T$  the temperature) of **1** is

Received: November 19, 2012

Published: March 21, 2013

shown in Figure 1. The thermal behavior of  $\chi T$  is typical of a two-step process, with a sharp transition at  $T_{1/2} \sim 142$  K,

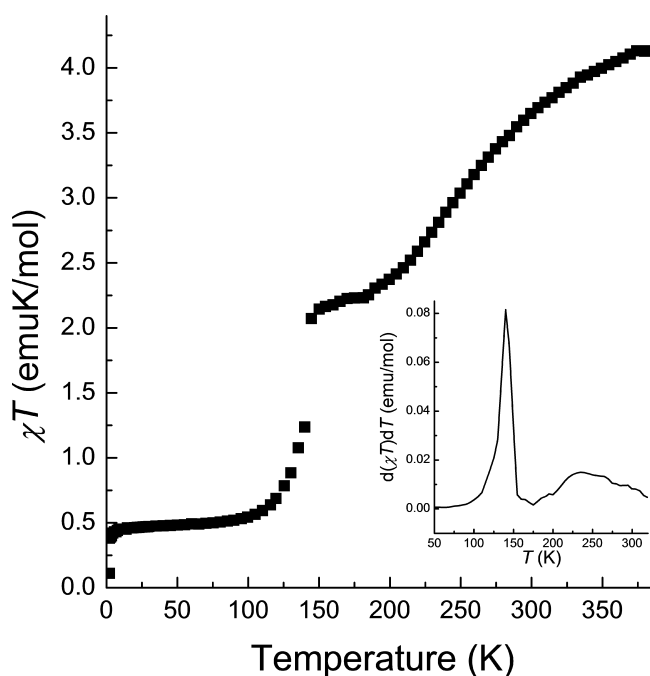


**Figure 1.**  $\chi T$  temperature dependence for **1**. The inset shows the first derivative of  $\chi T$  in the 50–380 K range.

separating the LS and an intermediate (Int) phase, and a gradual process at  $T_{1/2} \sim 250$  K, corresponding to the transition between the Int and the HS phases. At high temperatures,  $T > 365$  K, the  $\chi T$  is constant at  $\sim 4.10$  emu K mol<sup>-1</sup>, which is consistent with the expected value for Fe<sup>III</sup> in the HS state.<sup>6</sup> Upon cooling,  $\chi T$  decreases down to 220 K. Between 200 and 145 K, this decrease becomes slower, and  $\chi T$  remains nearly constant,  $\sim 2.2$  emu K mol<sup>-1</sup>. The value of  $\chi T$  in the plateau of the Int phase is only slightly below the calculated value for a 50:50 mixture of LS and HS Fe<sup>III</sup> centers,  $\chi T = \gamma\chi T_{\text{HS}} + (1 - \gamma)\chi T_{\text{LS}} = 2.52$  emu K mol<sup>-1</sup> (where HS fraction  $\gamma = 0.5$ ;  $\chi T_{\text{HS}} = 4.10$  emu K mol<sup>-1</sup>, and  $\chi T_{\text{LS}} = 0.46$  emu K mol<sup>-1</sup>). The HS fraction obtained from  $\chi$  measurements in this plateau (145–200 K) is  $\gamma \sim 0.48$ . As the temperature decreases,  $\chi T$  drops drastically. Finally, below 100 K,  $\chi T$  remains nearly constant at  $\sim 0.46$  emu K mol<sup>-1</sup>, which is consistent with the value expected for LS Fe<sup>III</sup>.<sup>7</sup> A full conversion from HS to LS Fe<sup>III</sup> is thus observed in the temperature range of 100–360 K. The temperature dependence of  $d\chi T/dT$  is shown in the inset of Figure 1, and the two maxima, at 142 (sharp peak) and  $\sim 250$  K (broad maxima), correspond to the two SCO processes. The low temperature one is a sharp process, while the second at higher temperatures seems rather sluggish and is complete only at quite high temperatures of  $\sim 360$  K. The magnetic susceptibility measurements obtained on cooling overlap rather well those obtained on warming, and there is no evidence of hysteresis. The approximately constant value of  $\chi T$ , at low temperatures, indicates that the magnetic interactions must be rather weak and, unlike other compounds, the role of magnetic interactions in the SCO processes of **1** may be neglected.

The Mössbauer spectra of **1** between 4 and 90 K show a quadrupole doublet with sharp peaks (see Supporting Information, Figure S1). The estimated isomer shift relative

to  $\alpha$ -Fe at room temperature, IS, and quadrupole splitting, QS (Table 1), are typical of LS Fe<sup>III</sup> with  $S = 1/2$ .<sup>5d,8,9</sup> The

**Table 1.** Estimated Parameters from the Mössbauer Spectra of **1**

T (K)	spin state <sup>a</sup>	IS (mm/s) <sup>b</sup>	QS (mm/s) <sup>c</sup>	$I_{\text{LS}}$ (%), <sup>d</sup> $I_{\text{HS}}$ (%)
295	LS	0.12	2.28	12
	HS	0.36	0.55	88
260	LS	0.14	2.43	36
	HS	0.43	0.50	64
240	LS	0.15	2.62	59
	HS	0.45	0.50	41
215	LS	0.17	2.73	71
	HS	0.47	0.43	29
200	LS	0.18	2.77	71
	HS	0.51	0.50	29
185	LS	0.19	2.78	77
	HS	0.53	0.55	23
155	LS	0.20	2.79	80
	HS	0.54	0.50	20
125	LS	0.21	2.80	96
	HS	0.51	0.53	4
100	LS	0.22	2.83	100
4	LS	0.23	2.88	100

<sup>a</sup>LS and HS, low spin ( $S = 1/2$ ) and high spin ( $S = 5/2$ ) Fe<sup>III</sup>. <sup>b</sup>IS isomer shift relative to metallic  $\alpha$ -Fe at 295 K. <sup>c</sup>QS quadrupole splitting. <sup>d</sup> $I_{\text{LS}}$ ,  $I_{\text{HS}}$  relative areas of HS and LS Fe<sup>III</sup>. Estimated errors are  $\leq 0.02$  mm/s for IS and QS;  $\leq 2\%$  for  $I_{\text{LS}}$  and  $I_{\text{HS}}$ , for  $I_{\text{LS}}$  and  $I_{\text{HS}}$ , except at 260 and 295 K where the uncertainties are  $\leq 8\%$ .

asymmetry of this doublet, due to slightly different relative areas of both lines, is often observed when crystals used to prepare the Mössbauer absorber have a particular cleavage. The particles obtained after powdering retain a geometrical shape that gives rise to preferred orientation effects.

In the 155–295 K range, in addition to the LS doublet, a broad absorption peak centered at  $\sim 0.50$  mm/s is observed, typical of HS Fe<sup>III</sup> with  $S = 5/2$ .<sup>5d,8,9</sup> The broad lines of HS Fe<sup>III</sup> may be explained by relaxation effects. Due to the negligible magnetic orbital moment of Fe<sup>III</sup> with  $S = 5/2$ , its paramagnetic relaxation time should be much lower than that of LS Fe<sup>III</sup>.<sup>5d,10,11</sup> The Mössbauer spectra of **1** at 295, 215, and 125 K, in the HS, Int, and LS phases, respectively, are shown in Figure 2.

The thermal dependence of the estimated relative areas for the HS Fe<sup>III</sup> doublet,  $I_{\text{HS}}$  (see Supporting Information, Figure S2), shows a trend similar to that observed for the HS Fe<sup>III</sup> fraction deduced from magnetization measurements. Below 125 K, all the Fe<sup>III</sup> is in a LS state ( $I_{\text{HS}} = 0\%$ ). At 125 K, a small absorption around 0.5 mm/s may be attributed to HS Fe<sup>III</sup> representing less than 5% of the total absorption area ( $I_{\text{HS}} < 5\%$ ). Between 125 and 155 K,  $I_{\text{HS}}$  increases  $\sim 16\%$ . Between 155 and 215 K, the increase in  $I_{\text{HS}}$  is slow, but above 215 K, it becomes again much steeper. The magnetic behavior of the sample of **1** that used to obtain Mössbauer spectra was observed to be similar to the one described previously (Figure 1), only the transition at  $T_{1/2} \sim 142$  K is smoother, and the plateau corresponding to the Int phase is not so well-defined (see Supporting Information, Figure S3). The discrepancy from the HS fraction,  $\gamma$ , deduced from the magnetization measurements and the Mössbauer spectra, in the Int phase plateau (250–150 K) seems to result from two contributions: the lower

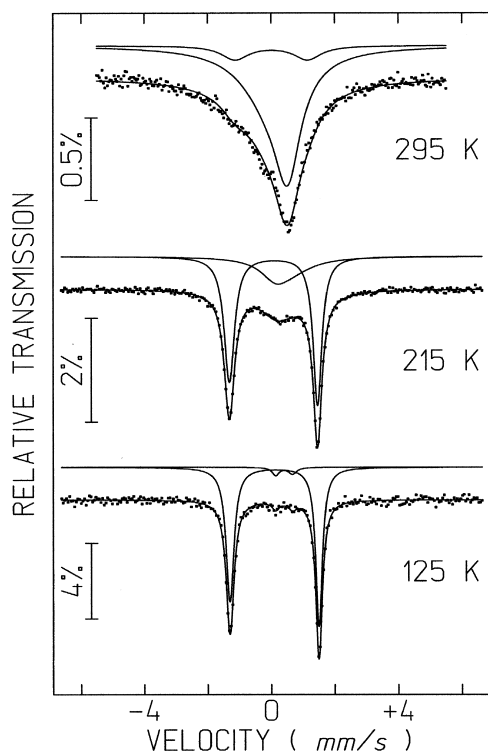


Figure 2. Mössbauer spectra of **1** at 125, 215, and 295 K.

crystallinity of the sample used to obtain the Mössbauer spectra (see Figures S2 and S3, in Supporting Information) and the difference in the Mössbauer recoil-less factors from the HS and LS Fe<sup>III</sup> centers. In general, due to the shorter and stronger Fe–ligand chemical bonds in the LS Fe<sup>III</sup> molecules, the recoil-less fractions of these Fe<sup>III</sup> species are higher than those of the HS Fe<sup>III</sup>, particularly above 80 K. Consequently, the estimated *I* for LS Fe<sup>III</sup> may be higher than the actual fraction of Fe<sup>III</sup> in the LS state.<sup>9</sup> In addition, close to room temperature, the large widths

of the Mössbauer absorption peaks of the title compound lead to high uncertainties in the estimated *I*. In this sense, the HS fraction deduced by the magnetic measurements seems more reliable than those inferred by the Mössbauer spectra, which is confirmed by the single crystal diffraction results (see below).

The crystal structures of **1** were determined by single crystal X-ray diffraction at 294, 150, and 50 K, in the HS, Int, and LS phases, respectively (the crystal data and refinement details are shown in Table 2). At room temperature, the asymmetric unit contains one [Fe(nsal<sub>2</sub>trien)]<sup>+</sup> cation and one SCN<sup>−</sup> anion. The analysis of the structure revealed distorted octahedral Fe<sup>III</sup>N<sub>4</sub>O<sub>2</sub> environments resulting from the coordination of the hexadentate nsal<sub>2</sub>-trien Schiff-base ligands to the Fe<sup>III</sup> centers (bond lengths of the Fe<sup>III</sup> coordination are summarized in Table 3 and Table S1 in the Supporting Information). The Fe–

Table 3. Fe<sup>III</sup> Coordination Bond Lengths [Å] at 50, 150, and 294 K

	294 K	150 K [Fe1]	150 K [Fe2]	50 K
	HS	HS	LS	LS
Fe–O	1.901(2)	1.905(2)	1.8782(18)	1.8843(18)
Fe–O	1.917(2)	1.9187(19)	1.8795(18)	1.8886(18)
Fe–N <sub>imine</sub>	2.051(3)	2.052(2)	1.909(2)	1.911(2)
Fe–N <sub>imine</sub>	2.052(3)	2.052(2)	1.929(2)	1.926(2)
Fe–N <sub>amine</sub>	2.131(3)	2.128(2)	2.000(2)	2.003(2)
Fe–N <sub>amine</sub>	2.154(3)	2.146(2)	2.022(2)	2.019(2)

N<sub>amine</sub>, Fe–N<sub>imine</sub>, and Fe–O bond lengths (where Fe–N<sub>amine</sub> > Fe–N<sub>imine</sub> > Fe–O) are comparable to those found for similar Fe<sup>III</sup> HS complexes.<sup>12</sup> In the structure obtained at 150 K (Int phase), there is a doubling of the unit cell that remains monoclinic (*Z* = 8 in the Int phase, while *Z* = 4 in the HS and LS phases), and it includes two crystallographically distinct cations and anions (see Figure 2). One cation [Fe1] reveals a similar distortion around the Fe<sup>III</sup> centers, with comparable values for the coordination bond lengths typical of HS Fe<sup>III</sup>

Table 2. Crystallographic Data for Compound **1** (at 50, 150, and 294 K)

	temperature (K)		
	294	150	50
cryst size (mm)	0.52 × 0.38 × 0.10	0.40 × 0.32 × 0.10	0.40 × 0.20 × 0.06
cryst color, shape	black, plate	black, plate	black, plate
formula	C <sub>29</sub> H <sub>28</sub> FeN <sub>5</sub> O <sub>2</sub> S	C <sub>29</sub> H <sub>28</sub> FeN <sub>5</sub> O <sub>2</sub> S	C <sub>29</sub> H <sub>28</sub> FeN <sub>5</sub> O <sub>2</sub> S
molecular mass	566.47	566.47	566.47
cryst syst	monoclinic	monoclinic	monoclinic
space group (no.)	<i>P</i> 2 <sub>1</sub> / <i>c</i>	<i>P</i> 2 <sub>1</sub> / <i>c</i>	<i>P</i> 2 <sub>1</sub> / <i>c</i>
<i>a</i> (Å)	13.468(6)	15.1175(9)	13.1705(2)
<i>b</i> (Å)	15.803(4)	15.6692(11)	15.6419(2)
<i>c</i> (Å)	15.366(7)	21.4295(15)	15.0038(2)
$\beta$ (°)	126.04(3)	90.282(3)	125.999(1)
<i>V</i> (Å <sup>3</sup> )	2644.6(2)	5076.1(6)	2500.67(6)
<i>Z</i> , <i>D</i> <sub>calcd.</sub> (Mg/m <sup>3</sup> )	4, 1.423	8, 1.482	4, 1.505
$\mu$ (mm <sup>−1</sup> )	0.686	0.715	0.726
<i>F</i> (000)	1180	2360	1180
$\theta$ range (deg)	2.58–25.68	2.67–25.03	2.6–25.68
index range ( <i>h</i> , <i>k</i> , <i>l</i> )	−16/15, 0/19, −18/15	−17/16, −18/18, −25/25	−16/13, −19/18, −17/18
reflns collected/unique	5241/5017 [R(int) = 0.0330]	45892/8950 [R(int) = 0.0554]	15631/4727 [R(int) = 0.0656]
<i>T</i> max./min.	0.9472/0.7168	0.9319/0.7630	0.9578/0.7601
goodness-of-fit on <i>F</i> <sub>2</sub>	1.049	1.054	1.077
final R1, [ <i>I</i> > 2 $\sigma$ ( <i>I</i> )], wR2	0.0536/0.1253	0.0421/0.1000	0.0476/0.01249

complexes. In the other cation [Fe2], the octahedral distortion is slightly reduced and displays inferior values for the coordination bond lengths, which are consistent with those reported for LS Fe<sup>III</sup> complexes.<sup>12</sup> At 50 K, the crystal structure is isostructural to one observed at room temperature, displaying again one cation and one anion in the asymmetric unit. The coordination around the Fe<sup>III</sup> centers is similar to the one observed for the LS Fe<sup>III</sup> centers from the Int phase [Fe2]. The thermal contractions of the coordination bond lengths associated with the SCO processes (comparing the 294 and 50 K structures) are 1.3, 6.4, and 6.3% for the Fe–O, Fe–N<sub>imine</sub>, and Fe–N<sub>amine</sub> distances, respectively. At 150 K, the coordination bond lengths of the LS Fe<sup>III</sup> centers are identical (within the error margins) to the ones observed for the LS phase. For the HS Fe<sup>III</sup> centers, those distances are very similar to the ones of the HS phase, and only a slight contraction (of the order of 0.4%) was observed for the Fe–N<sub>amine</sub> separation. This indicates that at 150 K, the HS and LS populations must be ~50:50 in agreement with the magnetization measurements.

Despite the structural transitions, the supramolecular arrangement remains similar in the three phases. In the crystal structures, the shorter intermolecular contacts involve cation–anion contacts that give rise to an arrangement of parallel zigzag chains (with alternating anions and cations) along [0 1 0], as shown in Figure 3. In the Int phase, the HS and LS Fe<sup>III</sup> centers belong to distinct chains. The intrachain Fe–Fe separations are 8.663 and 8.937 Å in the LS and HS phases, respectively, while in the Int phase these separations are 8.658 and 8.887 Å for the LS and HS chains, respectively. Within the chains, the cation–anion separations were observed to be shorter for the LS than for the HS phases; for the Int phase, these separations lie between those found for the HS and LS phases. These contacts involve a S atom from the anion and a H<sub>amine</sub> from the sal<sub>2</sub>-trien ligand, and they correspond to separations of 2.416 and 2.482 Å (in LS) and 2.431 and 2.483 Å (LS chain in Int) and 2.485 and 2.522 Å (HS chain in Int) and 2.542 and 2.578 Å (in HS). Short contacts between cations in neighboring chains (CH...C) were observed in the three phases, with separations of 2.718, 2.603, and 2.632 Å for the HS, LS, and Int phases, respectively. The interacting chains form layers parallel to *bc*, for the LS and HS phases, or to *ab*, for the Int phase. In this phase (Int), the layers consist of alternating chains based on HS and LS Fe<sup>III</sup> centers (see Supporting Information, Figure S4). The interchain (within the layers) Fe–Fe separations are 7.511 and 7.690 Å for the LS and HS phases, and in the Int phase the Fe–Fe separations between parallel LS and HS chains alternate from 7.387 to 7.754 Å. Although not as short as the intralayer cation–cation and anion–cation (intrachain) contacts, several cation–cation short contacts (C...C, CH...C, CH...O, and CH...HC) involving cations from neighboring layers are present, thus giving rise to a 3D connectivity between the (HS or LS) Fe<sup>III</sup> centers. Unlike other similar compounds, no  $\pi\pi$  contacts were detected in **1**.

These results reveal the existence of a very rare situation with a sequence of phases HS, Int, LS, so-called “re-entrant,” in the sense that the high temperature crystal structure is recovered in the LS phase (isostructural to the HS phase), with an intermediate ordered (Int) phase. This behavior was previously found in [Fe<sup>II</sup>(2-pic)3]Cl2·EtOH.<sup>5a</sup> However, unlike the case of this compound, where the intermediate ordered state seems to result from the competition between local short-range magnetic interactions and long-range elastic interactions, a distinct situation is expected for **1**, as the magnetic interactions

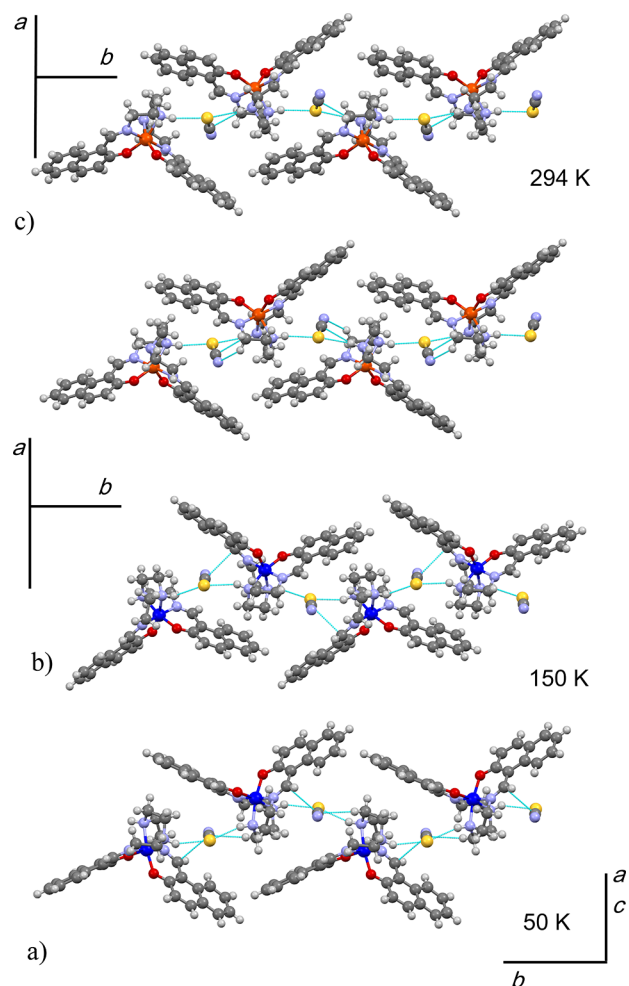


**Figure 3.** Projection of the crystal structure of **1** at 294, 150, and 50 K (in a, b, and c, respectively), showing the intermolecular arrangements of the anion–cation chains. The Int phase includes two chains (in b), one with HS and a second with LS Fe<sup>III</sup> (HS Fe atoms in orange and LS in blue).

between the Fe<sup>III</sup> centers seem to be very weak. In this case, as in other Fe<sup>III</sup> based two-step SCO systems, this behavior must be related with the existence of structural constraints preventing the full conversion to LS in a single step.<sup>5d</sup> Two-step SCO behaviors are known for a variety of Fe<sup>II</sup> complexes. This situation is quite rare for Fe<sup>III</sup> complexes, and symmetry breaking spin states in Fe<sup>III</sup> complexes were only observed in another case prior to **1**. With this compound, nevertheless, the determination of the crystal structures of the three phases (HS, Int and LS) was accomplished for the first time.

In order to ensure the absence of additional phases in the sample of compound **1** used for the magnetization and Mössbauer spectroscopic studies, an X-ray powder diffraction pattern was obtained at 294 K and compared with the powder pattern simulated from the single crystal data of **1**. A good agreement was observed between both patterns (see Supporting Information, Figure S5).

## CONCLUSIONS

The magnetization thermal dependence of compound **1** shows that at high temperatures this compound is HS and on cooling presents a behavior typical of two-step SCO, with two well separated spin transitions, one occurring gradually at ~250 K

and a second abruptly at 143 K. None of these transitions shows thermal hysteresis. The two-step SCO behavior was confirmed by Mössbauer spectroscopy in the range 4–295 K. Single crystal diffraction revealed the existence of an intermediate ordered phase with two crystallographic distinct Fe<sup>III</sup> centers (one HS and another LS), separating the isostructural HS and LS phases, each with a single Fe<sup>III</sup> center. The SCO behavior of compound **1**, particularly the sequence of phases ([HS]; [HS–LS]; [LS]) and the structural symmetry breaking in the intermediate ordered phase, as well as the “re-entrant” LS phase, is unique among Fe<sup>III</sup> compounds. A similar behavior was only previously found in [Fe<sup>II</sup>(2-pic)3]·Cl<sub>2</sub>·EtOH.<sup>5a</sup> In compound **1**, the magnetic interactions seem to be rather weak, and the origin of the two-step SCO process must be related with the existence of structural constraints preventing HS ↔ LS conversion in one step, unlike many Fe<sup>II</sup> based materials, where the magnetic interactions seem to play an important role in the appearance of a similar intermediate phase.<sup>13</sup>

## EXPERIMENTAL DETAILS

**Synthesis of 1.** A methanolic solution (30 mL) of 2-hydroxy-1-naphthaldehyde (10 mmol, 1721.80 mg) was added dropwise to a methanolic solution (30 mL) of triethylenetetramine (5 mmol, 731.17 mg). The yellowish mixture was stirred at reflux temperature for 30 min. Then, a solution of sodium methoxide (10 mmol, 540.24 mg) in methanol (10 mL) was added to the mixture, turning its color to orange. After 30 min of stirring, iron(III) chloride (5 mmol, 811.012 mg) dissolved in methanol (30 mL) was added dropwise, and the mixture turned black. Then, the volume was reduced to 40 mL, and 60 mL of dichloromethane was added. The solution was filtered, and a rotary evaporator was used to remove all of the solvent. The recovered precursor [Fe(nsald<sub>2</sub>t<sub>2</sub>)Cl] (4.956 mmol, 2695.14 mg) was then solubilized in 250 mL of water, at room temperature, and filtered. To the resulting filtrate was added dropwise a solution of KSCN (14.868 mmol, 1444.90 mg). The resulting solution was stored at 4 °C overnight. A colorless solution was recovered with a dark green deposit on the bottom, retrieved by filtration and washed with diethyl ether. The gathered solid was dried under vacuum conditions for 24 h at 80 °C. Yield: 2695.16 mg (96%). Elem Anal. Calcd: C, 61.49; H, 4.98; N, 12.36; S, 5.66%. Found: C, 61.47; H, 4.98; N, 12.36; S, 5.64%. Dark green crystals were obtained via slow evaporation of diethyl ether of a concentrated solution of acetonitrile.

Magnetic measurements were performed on an S700X SQUID magnetometer with a 7 T magnet (Cryogenic Ltd.) and a SQUID MPS magnetometer with a 5.5 T magnet with polycrystalline samples. The temperature dependence of the magnetic susceptibility in the temperature range 5–380 K was measured under a magnetic field of 1 T. The paramagnetic susceptibility was obtained from the experimental magnetization data after correction for the sample holder contribution and diamagnetism (from tabulated Pascal constants).

Mössbauer spectra were collected in transmission mode using a conventional constant-acceleration spectrometer and a 25 mCi <sup>57</sup>Co source in a Rh matrix. The velocity scale was calibrated using α-Fe foil. The absorber was obtained by gently packing single crystals of **1** into a perspex holder (~4 mg/cm<sup>2</sup> of natural Fe). Low-temperature spectra were collected using a bath cryostat with the sample immersed in liquid He for measurements at 4.1 K, or by using flowing He gas to cool the sample above 4.1 K. The spectra were fitted to Lorentzian lines using a nonlinear least-squares method.<sup>14</sup> Isomer shifts (see Table 1) are given relative to metallic α-Fe at room temperature.

Due to the detected sequence of phases, we intended to collect the diffraction data (at 294, 150, and 50 K) using the same crystal. However, after obtaining the data at 294 K (approximate crystal dimensions: 0.52 × 0.38 × 0.10 mm<sup>3</sup>), this crystal was cleaved, and we used a smaller crystal fragment to obtain the data at 150 K

(approximate crystal dimensions: 0.40 × 0.32 × 0.10 mm<sup>3</sup>). This crystal was lost, and the data at 50 K were collected using a second crystal (approximate crystal dimensions: 0.40 × 0.20 × 0.06 mm<sup>3</sup>). Diffraction data for 294 K were collected on an Enraf–Nonius CAD 4 diffractometer [Mo Kα radiation (0.71073 Å)] operating in the ω–2θ mode. Empirical absorption correction (ψ scans)<sup>15</sup> was applied, and data reduction was performed with the WINGX<sup>16</sup> suite of programs. Diffraction data for 150 and 50 K were acquired with a Bruker AXS APEX CCD diffractometer [Mo Kα radiation source (λ = 0.71073 Å)], equipped with an Oxford Cryosystems low temperature device, in the ψ and ω scans mode. A semiempirical absorption correction was carried out using SADABS.<sup>17</sup> Data collection, cell refinement, and data reduction were done with the SMART and SAINT programs.<sup>18</sup> The structures were solved by direct methods with SIR97<sup>19</sup> and refined by full-matrix least-squares analysis with the SHELXL97<sup>20</sup> program using the WINGX software package.<sup>15</sup> Non-hydrogen atoms were refined with anisotropic thermal parameters, whereas H-atoms were included at idealized positions (crystal data and refinement details are summarized in Table 2). The CCDC reference numbers are 911218 (50 K), 891463 (150 K), and 911217 (294 K).

## ASSOCIATED CONTENT

### Supporting Information

Additional figures and tables (including details from Mössbauer and crystallographic data). CCDC reference numbers 911218 (50 K); 891463 (150 K) and 911217 (294 K). This material is available free of charge via the Internet at <http://pubs.acs.org>.

## AUTHOR INFORMATION

### Corresponding Author

\*Tel: 351-21 994-6181. Fax: 351-21 955 0117. E-mail: [vascog@itn.pt](mailto:vascog@itn.pt)

### Notes

The authors declare no competing financial interest.

## ACKNOWLEDGMENTS

This work was partially supported by “Fundação para a Ciência e Tecnologia” (Portugal) under contract PTDC/QUI/65379/2006 and grant SFRH/BD/65237/2009.

## REFERENCES

- (1) (a) König, E. *Struct. Bonding (Berlin)* **1991**, 76, 51. (b) Kahn, O. *Molecular Magnetism*; Wiley-VCH: New York, 1993. (c) Gülich, P.; Garcia, Y.; Spiering, H. In *Magnetism: Molecules to Materials IV* Miller, J. S., Drillon, M., Eds.; Wiley-VCH: Weinheim, Germany, 2002; pp 271–344; (d) Gülich, P.; Goodwin, H. A. *Spin Crossover in Transition Metal Compounds I–III. Top. Curr. Chem.*; Springer: Berlin, 2004; pp 233–235.
- (2) (a) Bousseksou, A.; Molnar, G.; Matouzenko, G. *Eur. J. Inorg. Chem.* **2004**, 4353. (b) Gülich, P.; van Koningsbruggen, P. J.; Renz, F. *Struct. Bonding (Berlin)* **2004**, 107, 27. (c) Real, J. A.; Gaspar, A. B.; Muñoz, M. C. *Dalton Trans.* **2005**, 2062. (d) Gaspar, A. B.; Ksenofontov, V.; Seredyuk, M.; Gülich, P. *Coord. Chem. Rev.* **2005**, 249, 2661. (e) Sato, O.; Tao, J.; Zhang, Y.-Z. *Angew. Chem., Int. Ed.* **2007**, 46, 2152. (f) Murray, K. S. *Aust. J. Chem.* **2009**, 62, 1081. (g) Brooker, S.; Kitchen, J. A. *Dalton Trans.* **2009**, 7331. (h) Koudriavtsev, A. B.; Linert, W. *J. Struct. Chem.* **2010**, 51, 335.
- (3) (a) Kahn, O.; Krober, J.; Jay, C. *Adv. Mater.* **1992**, 4, 718. (b) Kahn, O.; Martinez, C. J. *Science* **1998**, 279, 44. (c) Létard, J.-F.; Guionneau, P.; Goux-Capes, L. *Top. Curr. Chem.* **2004**, 235, 221. (d) Gaspar, A. B.; Muñoz, M. C.; Real, J. A. *J. Mater. Chem.* **2006**, 16, 2522.
- (4) (a) Garcia, Y.; Kahn, O.; Rabardel, L.; Chansou, B.; Salmon, L.; Tuchagues, J. P. *Inorg. Chem.* **1999**, 38, 4663. (b) Matouzenko, G. S.; Létard, J.-F.; Lecocq, S.; Bousseksou, A.; Capes, L.; Salmon, L.; Perrin, M.; Kahn, O.; Collet, A. *Eur. J. Inorg. Chem.* **2001**, 2935. (c) Hibbs, W.; van Koningsbruggen, P. J.; Arif, A. M.; Shum, W. W.; Miller, J. S. *Inorg.*

*Chem.* **2003**, *42*, 5645. (d) Poganiuch, P.; Decurtins, S.; Gütlich, P. *J. Am. Chem. Soc.* **1990**, *112*, 3270. (e) Hinek, R.; Spiering, H.; Schollmeyer, D.; Gütlich, P.; Hauser, A. *Chem.—Eur. J.* **1996**, *2*, 1427. (f) Weber, B.; Carbonera, C.; Desplanches, C.; Létard, J.-F. *Eur. J. Inorg. Chem.* **2008**, 1589. (g) Li, B.; Wei, R.-J.; Tao, J.; Huang, R.-B.; Zheng, L.-S.; Zheng, Z. *J. Am. Chem. Soc.* **2010**, *132*, 1558. (h) Klingele, J.; Kaase, D.; Klingele, M. H.; Lach, J.; Demeshko, S. *Dalton Trans.* **2010**, 1689. (i) Shongwe, M. S.; Al-Rashdi, B. A.; Adams, H.; Morris, M. J.; Mikuriya, M.; Hearne, G. R. *Inorg. Chem.* **2007**, *46*, 9558. (j) Wei, R.-J.; Li, B.; Tao, J.; Huang, R.-B.; Zheng, L.-S.; Zheng, Z. *Inorg. Chem.* **2011**, *50*, 1170.

(5) (a) Chernyshov, D.; Hostettler, M.; Tornroos, K. W.; Burgi, H.-B. *Angew. Chem., Int. Ed.* **2003**, *42*, 3825. (b) Bonnet, S.; Siegler, M. A.; Costa, J. S.; Molnar, G.; Bousseksou, A.; Spek, A. L.; Gameza, P.; Reedijk, J. *Chem. Commun.* **2008**, 5619. (c) Bréfuel, N.; Watanabe, H.; Toupet, L.; Come, J.; Matsumoto, N.; Collet, E.; Tanaka, K.; Tuchagues, J.-P. *Angew. Chem., Int. Ed.* **2009**, *48*, 9304. (d) Griffin, M.; Shakespeare, S.; Shepherd, H. J.; Harding, C. J.; Létard, J.-F.; Desplanches, C.; Goeta, A. E.; Howard, J. A. K.; Powell, A. K.; Mereacre, V.; Garcia, Y.; Naik, A. D.; Muller-Bunz, H.; Morgan, G. G. *Angew. Chem., Int. Ed.* **2011**, *50*, 896.

(6) Harding, D. J.; Sertphon, D.; Harding, P.; Murray, K. S.; Moubarak, B.; Cashion, J. D.; Adams, H. *Chem.—Eur. J.* **2013**, *19*, 1082.

(7) van Koningsbruggen, P. J.; Maeda, Y.; Oshio, H. *Top. Curr. Chem.* **2004**, *233*, 259.

(8) Nihei, M.; Shiga, T.; Maeda, Y.; Oshio, H. *Coord. Chem. Rev.* **2007**, *251*, 2606–2621.

(9) Clemente-León, M.; Coronado, E.; López-Jordà, M.; Espallargas, G. M.; Soriano-Portillo, A.; Waerenborgh, J. C. *Chem.—Eur. J.* **2010**, *16*, 2207.

(10) P. Gütlich, Link, R.; Trautwein, A. *Inorganic Chemistry Concepts 3: Mossbauer Spectroscopy and Transition Metal Chemistry*; Springer-Verlag: Berlin, 1978.

(11) Timken, M. D.; Abdel-Mawgoud, A. M.; Hendrickson, D. N. *Inorg. Chem.* **1986**, *25*, 160.

(12) (a) Pritchard, R.; Barrett, S. A.; Kilner, C. A.; Halcrow, M. A. *Dalton Trans.* **2008**, 3159. (b) Floquet, S.; Muñoz, M. C.; Rivière, E.; Clément, R.; Audière, J.-P.; Boillot, M.-L. *New J. Chem.* **2004**, *28*, 535. (c) Sinn, E.; Sirn, G.; Dose, E. V.; Tweedle, M. F.; Wilson, L. J. *J. Am. Chem. Soc.* **1978**, *100*, 3375. (d) Faulmann, C.; Szilágyi, P. Á.; Jacob, K.; Chahine, J.; Valade, L. *New J. Chem.* **2009**, *33*, 1268. (e) Dorbes, S.; Valade, L.; Real, J. A.; Faulmann, C. *Chem. Commun.* **2005**, 69.

(13) (a) Mikami, M.; Konno, M.; Saito, Y. *Chem. Phys. Lett.* **1979**, *63*, 566–569. (b) Sasaki, N.; Kambara, T. *Phys. Rev. B* **1989**, *40*, 2442. (c) Bousseksou, A.; Nasser, J.; Linares, J.; Boukhedden, K.; Varret, F. *J. Phys. I* **1992**, *2*, 1381. (d) Spiering, H.; Kohlhaas, T.; Romstedt, H.; Hauser, A.; Bruns-Yilmaz, C.; Gütlich, P. *Coord. Chem. Rev.* **1999**, *190–192*, 629–647.

(14) Rodrigues, J. V.; Santos, I. C.; Gama, V.; Henriques, R. T.; Waerenborgh, J. C.; Duarte, M. T.; Almeida, M. *Dalton Trans.* **1994**, 2655.

(15) North, A. C. T.; Phillips, D. C.; Mathews, F. S. *Acta Crystallogr.* **1968**, *A24*, 351.

(16) Farrugia, L. J. *J. Appl. Crystallogr.* **1999**, *30*, 837.

(17) Sheldrick, G. M. *SADABS*; Bruker AXS Inc.: Madison, WI, 2004.

(18) *SMART*; *SAINT*; Bruker AXS Inc.: Madison, WI, 2004.

(19) Altomare, A.; Burla, M. C.; Camalli, M.; Cascaro, G.; Giacovazzo, C.; Guagliardi, A.; Moliterni, A. G. G.; Polidori, G.; Spina, R. *J. Appl. Crystallogr.* **1999**, *32*, 115.

(20) Sheldrick, G. M. *SHELX97*; University of Gottingen: Gottingen, Germany, 1997.